An attempt to model Obstructive Sleep Apnea Syndrome: preliminary study

Franz Chouly[1], Annemie Van Hirtum[2], Xavier Pelorson[2], Yohan Payan[1], and Pierre-Yves Lagrée[3]

[1] TIMC Laboratory, UMR CNRS 5525 and Université Joseph Fourier, 38706 La Tronche, France. {Franz.Chouly,Yohan.Payan}@imag.fr
[2] Institut de la Communication Parlée, INPG and UMR CNRS Q5009, F-38031 Grenoble Cedex, France. {annemie, pelorson}@icp.inpg.fr
[3] Laboratoire de Modélisation en Mécanique, UMR CNRS 7607, B 162, Université Paris 6, 75252 Paris, France. pyl@ccr.jussieu.fr

Abstract. The presented research attempts to model the interaction between the pharyngeal walls and the respiratory airflow during an apneic episode. Continuum mechanics has been considered to describe the upper airway soft tissues and the fluid flow is described by applying a Boundary Layer theory. A numerical method which implies Finite Element meshing of the walls has been developed for solving the mechanical problem. Preliminary results are presented. The partial closure of the airway which occurs during an hypopnea or at the beginning of an apnea has been simulated. A first validation has been carried out, by means of a comparison between predictions of numerical simulations and the experimental data measured on an in-vitro setup. The prediction error has been estimated to be of order of 20 %. The influence of physical meaningful parameters accounting for the pharyngeal caliber and the stiffness of the walls has been studied. This predictive model is a first necessary step before application within a clinical context, for instance in a procedure of surgical planning.

1 Introduction

Obstructive Sleep Apnea consists in brief and periodic episodes of soft-tissue collapsus within the upper airway during sleep [3] [13] [27] [42] [31] [12]. Each partial or total collapsus is followed respectively by limitation (hypopnea) or total cessation (apnea) of respiratory airflow. It has become a major health care topic, affecting 2 % to 4 % of the adults [43] with many consequences such as excessive daytime sleepiness or hypertension [27].

A standard treatment against Obstructive Sleep Apnea is Continuous Positive Airway Pressure (CPAP) [40], as its efficiency has been clearly demonstrated [27]. However, this technique is shown as compelling and not accepted by all patients, namely due to irritation problems caused by the mask or due to inacceptance for psychological reasons. Thus, surgical approaches have emerged in parallel to CPAP. Tracheostomy [24] is no longer considered as it was too invasive. Uvulopalatopharyngoplasty (UPPP) [15] has proven to be insufficiently efficient [27]. Tongue advancement surgery (maxillo-mandibular and hyoïd suspension surgery) [11] [16] seems more efficient but not easily accepted by patients. Additionally, conservative treatments, such as weight loss or oral appliances, are alternatives both to CPAP and surgery [19].

The basic mechanisms of an obstructive sleep apnea are already known thanks to clinical observation and to medical imaging: it is caused by an interaction within upper airway between soft-tissue (tongue, soft palate) and respiratory airflow [3]. The most significative factors such as anatomy, soft-tissue compliance and neuromuscular activation have been object of several physiological studies (e.g. [12]), although their relative impact is still controversial [35]. Thus, advances in understanding sleep apnea led to improvement of treatments. This paper is a modest attempt in this direction. Complementary to in-vivo studies, physical models have been developed, and represent another way to investigate the phenomenon which is at the origin of an apneic episode.

From the point of view of physical modelling, the most widespread tool is the collapsible tube [38] [23] [22] [6] [36] [8]. Although quite illustrative, such model might be too simplistic for surgical planning purposes. Indeed, it is perfectly symmetrical along its main axis, whereas the upper airway geometry is strongly asymmetrical. Alternative theoretical models have been proposed such as those of Auregan and Meslier [2] and of Fodil and al. [14]: one [2] or two [14] linear compliant segments are in interaction with non-viscous (Bernoulli) or viscous (Poiseuille) flows.

They proved their ability to reproduce a great diversity of behaviours, among which apnea or hypopnea. Their main limitation stands in the assumption that the upper airway can be approximated using linear discrete compliant segments.

From the point of view of fluid mechanics, numerical simulations of fluid circulation in the rigid upper airway have also been proceeded [37], which are helpful to determine velocity profiles as well as the pressure forces applied on walls. Of course, they do not account for the flow structure interaction, which prevents them to be sufficient for prediction of an apnea. Finite Element models of fluid-structure interaction for sleep apnea have been recently published like the bidimensional model of Malhotra [26]. However, before such models could be used for clinical purpose, they ought to be validated through confrontation with experimental data.

The present research is another attempt to develop an accurate theoretical and predictive model for sleep apnea. It is based on a description of the soft tissue as a continuous media, for which equilibrium equations are solved using the Finite Element method. Boundary layer theory is used for the description of the fluid flow. Interaction between fluid and walls is taken into account thanks to an iterative algorithm. As it is very difficult to know *a priori* whether a numerical method will provide satisfactory results, especially for fluid-structure problems, comparison with experimental data is necessary. So, this model will be quantitatively validated against an in-vitro setup. Influence of mechanical parameters which have a physiological meaning will be studied. This preliminary step is necessary before creation of more realistic models that might be useful in a context of surgical planning.

2 Theoretical assumptions and methods

Assumptions and method for computing wall deformation are presented in (2.1), while the computation of the pressure distribution is detailled in (2.2). Obtainment of pressure forces that act on the walls is the object of a specific development in (2.3). Finally, the global procedure to take into account the interaction between fluid and walls is detailled in (2.4).

2.1 Description of the walls

Models for obstructive sleep apnea syndrome such as [2] or [14] consider the upper airway as one or two independant compliant segments, governed by equations of general form:

$$A_i = f(p_i), \tag{1}$$

where A_i is the sectionnal area of the fluid channel below the segment i and p_i is the transmural pressure at the level of the segment i. f is a state function. Assuming that the state function is linear, the segment acts like a spring and $f(x) = k^{-1}.x$, k is the stiffness coefficient of the spring. However, such simple description might not be sufficient to reproduce accurately the highly complex behaviour of the upper airway soft tissues, especially in perspective of a realistic prediction. A more appropriate representation of soft tissue would be to consider it as a continuous media, in which the relationship between local deformation and local constraint is computed everywhere. Local deformation is represented by a second-order tensor, for instance the Green-Lagrange tensor $\mathbf{E}$. Local constraint is reprented by the Cauchy stress tensor $\boldsymbol{\sigma}$, another second-order tensor[7].

As a result, continuum mechanics has been chosen as a framework for this study [7]. In addition, two assumptions have been formulated so as to simplify the mechanical problem. It is firstly supposed that inertia forces are negligible, which is a quasi-static assumption: both apnea and hypopnea involve slow tissue motions compared to those observed in speech or snoring. Assumption of small deformations is also stated: structure deformation from rest position is supposed not to exceed 15 %, so that second order terms can be dropped out in $\mathbf{E}$, to obtain the small deformations tensor $\boldsymbol{\varepsilon}$. Since material is supposed to be linear, isotropic and homogeneous, the elastic hookean law is sufficient to describe its constitutive properties:

$$\boldsymbol{\sigma} = \frac{E\nu}{(1-2\nu)(1+\nu)}\mathrm{tr}(\boldsymbol{\varepsilon})\mathbf{I} + \frac{E}{1+\nu}\boldsymbol{\varepsilon}, \tag{2}$$

where $\mathbf{I}$ is the identity tensor, $\mathrm{tr}(\boldsymbol{\varepsilon})$ is the first invariant of the small deformations tensor, E is the Young modulus, ν is the Poisson's ratio [4]. The Young modulus E (in Pa) is associated to material stiffness, and the Poisson's ratio ν is linked with compressibility. The closest to 0.5 ν is, the less compressible the material is.

For a model of the upper airway, complex repartition of boundary conditions, such as kinematic constraints and external forces distribution, prevents from solving the mechanical problem analytically. The chosen numerical tool for resolution is the Finite Element method, widely used in structural engineering and in biomechanics [44]. The geometry of the structure is approximated by a mesh, constituted of a finite number of nodes which delimit elements.

In structural analysis, once the mesh is defined, the best approximation of solution is obtained from determination of nodal displacements that minimize total potential energy of the structure: this variational formulation of an elasticity problem is detailled in [44]. From nodal displacements, values of small deformations tensor $\boldsymbol{\varepsilon}$ and of constraint tensor $\boldsymbol{\sigma}$ are established at each point of the structure as the aim of Finite Element method is to provide a continuous approximation. Under the assumption of small deformations, and with quasi-static hypothesis, it can be demonstrated [44] that requiered nodal displacements are obtained from solving a linear system:

$$[\mathbf{K}]\{\mathbf{u}\} = \{\mathbf{F}\}, \tag{3}$$

where $\{\mathbf{u}\}$ is the vector of nodal displacements [4], $\{\mathbf{F}\}$ is the vector of external forces applied to each node and $[\mathbf{K}]$ is the stiffness matrix, obtained from integration of the constitutive law (2) on

[4] each component of $\{\mathbf{u}\}$, if not constrained, is called a degree of freedom

each element [44]. Displacement vector is decomposed as following: $\{\mathbf{u}\} = \{\mathbf{u_f}\,\mathbf{u_c}\}^t$ where $\mathbf{u_f}$ is constituted of all degrees of freedom, and $\mathbf{u_c}$ of all constrained displacements. Obtention of $\{\mathbf{F}\}$ is detailled in 2.3.

$$\{\mathbf{u_f}\} = [\mathbf{M}]\,\{\mathbf{F}\} + \{\mathbf{u_f}^*\} \tag{4}$$

where $[\mathbf{M}]$ matrix is derived from the stiffness matrix $[\mathbf{K}]$ after simple algebra [20], and will be named the compliance matrix. $\{\mathbf{u_f}^*\}$ is a displacement vector induced by constant constraints in force and in displacement.

So as to compute the $[\mathbf{M}]$ matrix, a commercial finite element solver (Ansys(TM) Software) has been employed, which ensures high reliability and accuracy of computations. However, it does not allow straightforward computation of this matrix. So, a method similar than the one described in [9] permits to precompute the $[\mathbf{M}]$ and the $\{\mathbf{u_f}^*\}$ vector associated to elementary deformations. Furthermore, it avoids carrying complete structural analysis at each iteration of the main loop of the fluid-structure coupling algorithm. The precomputation method is described in Appendix 1.

2.2 Description of the airflow

Characteristics of flow circulation within a constriction have been studied extensively, for instance in the glottis [33] [32] [18] [29], in a stenosis [5] or in the pharynx [37]. From these studies, a schematic description of the flow is illustrated in figure 1. While entering in constriction, fluid particles are submitted to acceleration due to the constant flow rate. After the narrowest part of the constriction, fluid tends to decelerate and to separate from walls, to form a free jet (figure 1).

The choice of an adequate fluid model for pressure prediction is all the more important as it has a direct and significative impact on fluid-structure interactions. In [17], different models have been confrontated to experimental measurements on an in-vitro setup. Choice of the model described in this section results directly from this confrontation and is briefly described in the following.

Fluid model is derived from simplifications of the Navier-Stokes (5) and continuity (6) equations assuming a quasi-steady, incompressible, laminar and bidimensionnal flow:

$$(\boldsymbol{v}.\mathbf{grad}\,)\boldsymbol{v} = -\,\tfrac{1}{\rho}\,\mathbf{grad}\,P + \nu\nabla^2\boldsymbol{v}, \tag{5}$$

$$\mathrm{div}\,\boldsymbol{v} = 0, \tag{6}$$

where P is pressure, ρ is density, ν is kinematic viscosity, $\boldsymbol{v}$ is local velocity. With help of two other supplementary assumptions, which are channel transversal dimension h_0 smaller than its longitudinal dimension D (figure 1) and high Reynolds number $Re = U_0 h_0/\nu$ (U_0 is the mean longitudinal speed), the Navier-Stokes (5) and continuity (6) equations can be simplified so as to obtain Reduced Navier-Stokes / Prandtl equations [25] :

$$\bar{u}\frac{\partial\bar{u}}{\partial\bar{x}} + \bar{v}\frac{\partial\bar{u}}{\partial\bar{y}} = -\frac{\partial\bar{p}}{\partial\bar{x}} + \frac{\partial^2\bar{u}}{\partial\bar{y}^2}, \tag{7}$$

$$-\frac{\partial\bar{p}}{\partial\bar{y}} = 0, \tag{8}$$

$$\frac{\partial\bar{u}}{\partial\bar{x}} + \frac{\partial\bar{v}}{\partial\bar{y}} = 0, \tag{9}$$

where all variables are nondimensionnal : $\bar{x} = x(h_0 Re)^{-1}$, $\bar{y} = yh_0^{-1}$, $\bar{p} = P(\rho U_O^2)^{-1}$, $\bar{u} = uU_0^{-1}$, $\bar{v} = vReU_0^{-1}$. (u, v) are longitudinal and transversal components of velocity $\boldsymbol{v}$: [17], [25]. Boundary conditions consist in no slip on the lower and upper walls [17].

For a flow circulation within a constriction, RNS/P equations (7), (8), (9) are appropriate to describe the effects of viscosity, that concentrate on a thin layer upon walls: the boundary layer [34]. From the RNS/P equations, computation of wall shear stress τ_{wall} is possible and used as a criterion to determine position of fluid separation from walls, where it vanishes:

$$\tau_{wall} = \rho\nu \frac{\partial u}{\partial y}|_{y=y_{wall}} = 0, \tag{10}$$

The accuracy of such prediction has extensively been studied in [17], compared to other prediction theories such as 1D inviscid flow or 2D boundary layer.

This set of equations is solved using finite differences method with a regular grid [25], [10]. A vector $p(x_i^p)_{i=1,\dots,n_{max}}$, which represents pressure distribution all along a two-dimensionnal channel, is then obtained. $(x_i^p)_{i=1,\dots,n_{max}}$ is the abscissa of each grid point where pressure is computed.

2.3 Computation of pressure forces

As the fluid model is assumed to be bidimensionnal and the structural model is tridimensionnal, the structure is divided into slices of small thickness. From fluid simulation on each slice, a pressure distribution is stored for each element (fig. 2).

For an element (e), the only way to compute deformation from pressure distribution on the element surface S is to determine nodal forces equivalent to pressure. This is achieved by use of the virtual work theorem:

$$\left\{\mathbf{F}^{(e)}_{nodes}\right\} = \int_S [\mathbf{N}(\mathbf{x})]^t \, p(\mathbf{x}) \, \{\mathbf{n}(\mathbf{x})\} \, dS, \tag{11}$$

where $\left\{\mathbf{F}^{(e)}_{nodes}\right\}$ is the vector of equivalent nodal forces. For a point $\mathbf{x}$ in the surface S of (e), $[\mathbf{N}(\mathbf{x})]$ is the interpolation matrix, $p(\mathbf{x})$ is the pressure and $\{\mathbf{n}(\mathbf{x})\}$ is the normal vector to the surface element (fig. 3) [44], [7]. For a quadrilateral element of four nodes, with the standard local coordinate system (s,t) shown in fig. 4, expression (11) might be simplified in:

$$\left\{\mathbf{F}^{(e)}_{nodes}\right\} = \left(\int_{-1}^{1}\int_{-1}^{1}\left[\mathbf{N}(s,t)\right]^t p(s,t)dsdt\right)\frac{\{\mathbf{a}\}}{4}, \tag{12}$$

where

$$\mathbf{a} = (\mathbf{x}^{\mathbf{1}}_{\mathbf{-1}} - \mathbf{x}^{\mathbf{-1}}_{\mathbf{-1}}) \wedge (\mathbf{x}^{\mathbf{-1}}_{\mathbf{1}} - \mathbf{x}^{\mathbf{-1}}_{\mathbf{-1}}) \tag{13}$$

is the area vector associated to the element, $\mathbf{x}^{\mathbf{-1}}_{\mathbf{-1}}$, $\mathbf{x}^{\mathbf{1}}_{\mathbf{-1}}$, $\mathbf{x}^{\mathbf{1}}_{\mathbf{1}}$, $\mathbf{x}^{\mathbf{-1}}_{\mathbf{1}}$ being element nodes (fig. 4). For a discrete pressure distribution $p(s_i, t_j)_{i=1,\ldots,n,\, j=1,\ldots,m}$ associated to an appropriate subdivision $(s_i, t_j)_{i=1,\ldots,n+1,\, j=1,\ldots,m+1}$ of the element surface, it can be shown that for each node (k, l), where $k, l \in \{-1, 1\}$ stand for node of coordinates $\mathbf{x}^k_l$, equivalent force is:

$$\left\{\mathbf{F}^{k\,(e)}_l\right\} = \left(kl\sum_{i=1}^{n}\sum_{j=1}^{m} p(s_i, t_j)\omega(ks_i, ks_{i+1})\omega(lt_j, lt_{j+1})\right)\frac{\{\mathbf{a}\}}{16}, \tag{14}$$

with

$$\omega(x, y) = \frac{1}{2}(y - x)(1 + x + y). \tag{15}$$

Obtention of (14) is detailled in Appendix 2. Then, pressure force on each node of the mesh is the resultant of all the contributions of forces from adjacent elements, which allows to compute the vector $\{\mathbf{F}\}$ of external forces due to the fluid pressure (standard assembly procedure of Finite Element method).

2.4 A fluid-structure coupling algorithm

Both mechanical models of structure and fluid need to be in interaction. This is achieved by use of a general iterative fluid-structure coupling algorithm summarized in figure 5. Behaviour (structure deformation, flow characteristics) of the model is predicted for an initial condition : a given pressure drop ΔP between inlet and outlet of the fluid channel. It is increased step by step

: $\Delta P_1 = 0, \ldots, \Delta P_{n_{steps}} = \Delta P$ where n_{steps} is the number of steps.

For each step i, a given pressure drop ΔP_i is imposed. Geometry of the channel is obtained from the structure, after deformation at step $i-1$. Fluid model is then used to compute pressure distribution along the channel and thus forces applied to the walls, which deformation is predicted in response using the structure model. This deformation induces new boundary conditions. As a result, a new pressure distribution has to be computed from which a new walls deformation is obtained. The algorithm keeps on iterating until a fixed number of iterations $n_{iterations}$ is reached. With a correct choice for $n_{iterations}$, no significative difference between two successive deformations can be observed (convergence criterion) and equilibrium is then reached (quasi-steady hypothesis). Typically, a choice of $n_{iterations} = 5$ was found to be sufficient to ensure convergence. At the end of the loop, the step is increased from i to $(i+1)$.

3 In-vitro setup

The pharyngeal airway has a highly complex anatomical structure which can be roughly divided into main entities such as the tongue, the soft palate, the uvula and the pharyngeal walls. These soft tissues are mostly composed of muscles and fat deposits. Some bony structures are used as insertions for muscles: mandibulae, hard palate, hyoid bone. More than twenty upper airway muscles are thought to be influent on the diameter of pharyngeal lumen [3]. Thus, collapsus has been reported to occur in various pharyngeal segments. Sites of collapsus are mostly in oropharynx, posterior either to uvula or to radix linguae [30]. They correspond to local minima of pharyngeal sectionnal area, in other terms to constriction sites.

Though a very realistic anatomical and mechanical model of upper airway would be the best solution for accurate simulation, for the sake of simplicity, our modelling approach will be validated at first on an idealized geometry. So, the main goal of the in-vitro setup is to reproduce a fluid-structure interaction within a constriction, from which observations and measurements could be obtained in order to allow comparison with simulations predicted from the theoretical model. First, the in-vitro setup is briefly described in 3.1. Then, a Finite Element model of the deformable wall of the setup is presented in 3.2.

3.1 Description

The setup under study is depicted in figure 6. It consists of a cylinder attached to a rigid pipe, which delimits a channel for the airflow. In first approximation, the cylinder can be considered to play the role of the tongue and the rigid pipe to represent the trachea and the posterior pharyngeal wall (figure 6 (c)). The cylinder can either be rigid (metallic) or deformable (thin latex tube filled with water). The use of a rigid cylinder is an interesting first step as it allows very accurate mesures of fluid characteristics (velocity, pressure) which are fully described in [17]. The latex cylinder is used as a second step for observations of flow-induced deformation. The diameter D of the latex tube is 49 mm. The internal diameter d of the rigid pipe is 25 mm. The thickness l_t of the latex is 0.3 mm. Initial height h_c at the level of constriction is the main variable geometrical parameter (figure 6 (a)). A pressure tap was drilled in the rigid pipe upstream of the tongue replica in order to measure the pressure drop ΔP.

3.2 Finite Element model of the deformable wall

Within the framework described in (2.1), a Finite Element tridimensionnal model of the latex tube, which is the only deformable part of the in-vitro setup, has been designed, in agreement with both its geometry and its mechanical properties: constitutive mechanics and boundary conditions (figure 7 (a) (b)). Choice of a bidimensionnal model would have prevented from taking into account boundary conditions with fidelity. Poisson's ratio has been chosen as close as possible to 0.5 ($\nu = 0.499$) since latex is assumed to be perfectly incompressible. Water inside this thin latex wall has been taken into account by applying constant pressure forces on elements, which is consistent with the in-vitro setup. Kinematic constraints (immobility) have been chosen to be the nearest of those of the in-vitro setup (figure 7 (b))[5].

The model is built from hexahedra, which are three-dimensionnal eight nodes elements. Mesh regularity and good stability properties of hexahedra ensure a correct approximation of solution. As the Poissons's ratio value is imposed by imcompressibility, the only mechanical parameter of the model to fix is the Young modulus E.

4 Results and discussion

First, in (4.1), a method to determine the Young modulus E of the latex tube is exposed. Then, numerical simulations using the method described in (2) and the Finite Element model presented in (3.2) are carried out and compared to experiments in (4.2). Finally, the influence of the model parameters is discussed in (4.3).

4.1 Assessment of mechanical characteristics

Before proceeding to simulation of the fluid/wall interaction, the mechanical properties of the latex tube that belongs to the in-vitro setup have to be determined. It will ensure consistent comparisons in a second stage. In order to estimate the value of the Young modulus E, a preliminary experiment has been carried out. A complete experimental protocol of rheology measurement would have been necessary to evaluate E with accuracy. Yet, many of the existing protocols are not compatible with the specific configuration of the in-vitro setup. As a result, the method applied consisted in determining the wall deformation in response to the internal pressure variation induced by water, using simulation and experiment.

Experimentally, internal pressure P_{int} of the water inside the latex tube has been changed and measured. Deformation induced by this change has been evaluated through constriction height h_c

[5] as it can be visualized on figure 7, repartition of kinematic constraints on the cylinder inforce the choice of a tridimensionnal model.

in the middle section, which has been determined indirectly by measuring the intensity change of a laser beam. Calibration of the optical device was made against calibrated holes. Typical accuracy for h_c is of order of $10^{-2}mm$. No fluid flow was circulating within the rigid pipe ($\Delta P = 0$). The experimentally set initial conditions have been reproduced in simulations, by imposing constant forces on internal nodes, equivalent to a pressure P_{int} on surfaces of the elements. The constriction height $h_{c,num}$ after deformation in the middle section has been computed and compared to the experimental value $h_{c,exp}$.

In figure 8, both experimental and computed curves $h_c = h_c(P_{int})$ are superimposed. Note that for values of P_{int} higher than 2100 Pa, the latex tube is in contact with the floor of the rigid pipe and h_c is no longer decreasing. From the experimental curve, non-linear mechanical behaviour of the latex cylinder can be observed. Nevertheless, as a first approximation, the relationship might be linearized. The computed curves are linear, which is due to small deformations hypothesis and assumption of a linear relationship between constraint and deformation, with slope proportionnal to the inverse of the Young modulus E. Least square estimation leads to a value of the Young modulus $E \approx 1.6$ MPa. It is consistent with values for latex materials available in the literature [41].

4.2 Simulation of an hypopnea

In order to replicate the in-vitro behaviour of the latex wall in response to a fluid flow circulation, the following experiment has been realized: for a given value of the internal pressure P_{int} and of the initial constriction height h_c, a pressure drop ΔP has been imposed gradually between the inlet and the outlet of the rigid pipe. Evolution of the constriction height has been measured through intensity change of a laser beam (as explained in section 4.1). The relative deformation of the latex structure is evaluated through the quantity $\Delta h_c = (h_c^{init} - h_c^{def})/h_c^{init}$, where h_c^{init} is the initial height and h_c^{def} is the height after deformation. The deformation of the walls has been simulated, using the same parameters as those chosen for the experiment. A curve $\Delta h_{c,comp}(\Delta P)$

is then obtained, which allows quantitative comparison with the experimental data.

A typical example is illustrated in figure 9 for a constriction height h_c of 1.20 mm, a pressure drop ΔP of 200 Pa and an internal pressure P_{int} of 200 Pa. Another example is presented in figure 10 for a constriction height h_c of 0.87 mm, a pressure drop ΔP of 290 Pa, and an internal pressure P_{int} of 400 Pa. In both cases, 3 sets of experimental data corresponding to measurements made at different times, are compared to the numerical simulations. The general conclusions that can be drawn from this study are summarized as follows:

For an initial constriction height small enough, an increase of the pressure drop ΔP results into a decrease of h_c (hypopnea phenomenon). This relationship is observed and simulated to be approximately linear. The constriction height decrease is a natural consequence of the negative pressure forces at the level of constriction [17].

Compared with experimental data the simulations appear to be in reasonable agreement. Overall, typical discrepancies are of order of 20 % at the most which is quite satisfactory considering the amount of theoretical simplifications involved.

Experimentally it is observed that mechanical instabilities are observed when the pressure drop ΔP reaches a critical value. This critical value is a function of both the mechanical characteristics of the tongue replica and of the initial geometrical conditions. Typically these instabilities lead to self sustained oscillations which can't be simulated numerically due to the assumption of quasi-steadiness. From a pathological point of view such a situation would however correspond to snoring rather than apnoea.

4.3 Sensibility of the model to geometrical and mechanical parameters

In order to illustrate the potential usefullness of the simulation software, the influence of three important geometrical and mechanical parameters have been studied. The choice of these parameters is led by the physiological interpretation that can be done. These parameters are the initial constriction height, the Young modulus and the internal pressure of water inside the latex tube. The influence of all these parameters is evaluated through computation of relative constriction height variation Δh_c.

The first parameter investigated is the initial constriction height, which influence can be observed in figure 11. Simulations had been proceeded for a pressure drop ΔP of 150 Pa and an internal pressure P_{int} of 200 Pa. The higher is the value of the initial constriction height, and thus the wider is the channel, the less important is the pressure drop within the constriction.

In terms of obstructive sleep apnea, the constriction height corresponds to the minimal pharyngeal caliber, which is well known to be a critical anatomical factor, directly in relationship with the upper airway collapsus [12]. The result of figure 11 seems to be qualitatively in agreement with in-vivo and clinical observations. For instance, Isono & al. showed that the pharynx of apneic patients was narrower than the pharynx of a reference group [21]. Indeed, an increase of the pharyngeal caliber corresponds to a decrease of apnea or hypopnea frequency and severity. This explains the efficiency of surgical procedures that enlarge upper airway like maxillo-mandibular advancement [16] or oral appliances [19].

The second parameter examinated was the Young modulus E of the latex tube. Simulations where carried out with a pressure drop ΔP of 150 Pa, an internal pressure P_{int} of 200 Pa, an initial constriction height h_c of 1.5 mm. E has been chosen within a range of values that went from 0.4 MPa up to 2 MPa. The curve that shows incidence of E on variation of the constriction height has been plotted (figure 12). As the Young modulus is increased, the walls are more rigid and less influenced by the fluid flow pressure, which results in a less important collapsus. This is consistent with the findings of precedent numerical simulations [28]. This is also in agreement with the already mentionned study of Isono & al in which the pharynx has been found more collapsible in apneic patients than in normal subjects [21] [6].

Finally, the influence of internal pressure P_{int} has been investigated. This parameter is interesting as it modifies both the elasticity and the initial constriction height h_c at the same time. In physiological reality, input parameters are indeed seldom independent. Moreover, this study allows to check if the model response to a complex input is correct. Simulations had been carried out, for a pressure drop ΔP of 150 Pa and an initial constriction height h_c of 1.5 mm. The impact of varying the imposed internal pressure on the constriction height variation is depicted in figure 13. The curve shows a positive quasi-linear relationship between varying internal pressure and resulting variation in constriction height. Such a comportmental behaviour curve is of practical interest in clinical research as it allows to predict a critical pressure $P_{crit} \approx 1400$ Pa for which the channel would be closed (apnea).

5 Conclusion

A method for simulating the interaction between airflow and walls within the upper airway during an apneic episode has been described. A preliminary quantitative validation has been carried out based on comparison between predictions from numerical simulations and measurements on an in-vitro setup. Concerning the prediction of deformations the average error is of order of 20 indirect determinations that needed to be done. Further, simulation results were shown to be qualitatively consistent with medical and clinical observations, especially through the simulation of an hypopnea.

[6] and compliance of the pharynx has always been pointed out as an important mechanical factor of sleep apnea [12].

Of course the ultimate goal of this research project, build a validated physical model of Sleep Apnoea, is far to be achieved. In particular, in its present state, the simulations are basically limited to hypopnea effects for two reasons. The first one is due to the small deformations assumption as well as the assumption of a linear elastic Hook law which are probably both erroneous when a full collapse of the airways is involved. An hyperelastic law, within a framework of large deformations, might thus be more appropriate to simulate apnoea. A second theoretical problem occurs with the description of the contact between the soft tissues and the pharyngeal walls as is expected during a complete apnoea. Different theoretical solutions based on Hertz models [39] are currently investigated. Because of the strong nonlinearity induced, the collision model is expected to be of major importance for the validity of the simulations. It must be noted that during the closure of the airways the Boundary-Layer flow model is also subject to question. A fully viscous description fro the flow seems to be a better alternative.

A similar effort concerning the experimental validation of the simulations must be developed in parallel. In practice this involves measurements of two (or even three) dimensional deformations together with accurate fluid mechanical measurements. A set-up involving a digital camera coupled with pressure and velocity sensors is currently developed for this purpose. More realistic pharyngeal geometry need of course to be considered although, concerning in-vitro experiments, the design, the realization and the control of complex geometries is quite challenging. Concerning the simulations however, and in view of clinical application, the specific anatomical and biomechanical properties of upper airway soft tissues can be considered in a less simplistic manner. A first important step will be to build models from imaging datasets such as x-ray bidimensionnal sagittal radiographies or CT-scans. Therefore, the anatomy of apneic patients could be accurately taken into account. Then, the complex properties observed on muscular and fat tissues such as inhomogeneity or anisotropy should be integrated in the elastic law, in addition to values measured from in-vivo rheological experiments. Then, such models might be of interest for the planning procedure of surgery.

Acknowledgements

The authors would like to thank Alice Perret, Jacques Ohayon and Pascal Swider for their comments and contributions. They would like to thank also the "Ministère de l'Enseignement Supérieur et de la Recherche" for having supporting this work. The work is part of an Emergence project granted by the CNRS federations ELESA/IMAG and the Rhône-Alpes region, France.

References

1. Ansys. *Theory Reference*, 2002. Release 6.1.
2. Y. Auregan and N. Meslier. Modélisation des apnées obstructives du sommeil. *Comptes-Rendus de l'Académie des Sciences, Série II*, 316:1529–1534, 1993.
3. I. Ayappa and D.M. Rapoport. The upper airway in sleep : physiology of the pharynx. *Sleep Medicine Reviews*, 7(1):9–33, 2003.
4. D. Bellet and J.J. Barrau. *Cours d'Elasticité*. Cepadues Editions - Collection La Cheveche, 1990. ISBN : 2.85428.245.0.
5. S.A. Berger and L-D Jou. Flows in stenotic vessels. *Annu. Rev. Fluid Mech.*, 32:347–382, 2000.
6. C.D. Bertram and T.J. Pedley. A Mathematical Model of Unsteady Collapsible Tube Behaviour. *J. Biomechanics*, 15(1):39–50, 1982.
7. J. Bonet and R.D. Wood. *Nonlinear continuum mechanics for finite element analysis*. Cambridge University Press, 1997.
8. W.A. Conrad. Pressure-Flow Relationships in Collapsible Tubes. *IEEE Transactions On Bio-Medical Engineering*, 16(4):284–295, October 1969.
9. S. Cotin, H. Delingette, and N. Ayache. Real-Time Elastic Deformations of Soft Tissues for Surgery Simulation. *IEEE Transactions On Visualization And Computer Graphics*, 5(1):62–73, January-March 1999.
10. J. Cousteix. *Couche Limite Laminaire*. Editions Cépaduès, 1988.
11. L. Crampette, B. Carlander, M. Mondain, M. Billiard, B. Guerrier, and Y. Dejean. Surgical Alternatives to Uvulopalatopharyngoplasty in Sleep Apnea Syndrome. *Sleep*, 15(6):S63–S68, 1992.
12. P.C. Deegan and W.T. McNicholas. Pathophysiology of obstructive sleep apnoea. *European Respiratory Journal*, 8:1161–1178, 1995.
13. W. Ward Flemons. Obstructive Sleep Apnea. *The New England Journal Of Medicine*, 347(7):498–504, August 2002.
14. R. Fodil, C. Ribreau, B. Louis, F. Lofaso, and D. Isabey. Interaction between steady flow and individualised compliant segments: application to upper airways. *Medical and Biological Engineering and Computing*, 35:1–11, 1997.
15. S. Fujita, W. Conway, F. Zorick, and T. Roth. Surgical Correction of Anatomic Abnormalities in Obstructive Sleep Apnea Syndrome : Uvulopalatopharyngoplasty. *Otolaryngol Head Neck Surg*, 89:923–934, Nov-Dec 1981.
16. C. Guilleminault, M.A. Quera-Salva, N.B. Powell, and R.W. Riley. Maxillo-mandibular surgery for obstructive sleep apnoea. *Eur Respir J.*, 2:604–612, 1989.
17. A. Van Hirtum, X. Pelorson, and P.Y. Lagrée. In-vitro validation of some flow assumptions for the prediction of the pressure distribution during obstructive sleep apnea. *Medical and Biological Engineering and Computing*, in press.
18. G.C.J. Hofmans, G. Groot, M. Ranucci, G. Graziani, and A. Hirschberg. Unsteady flow through in-vitro models of the glottis. *J. Acoust. Soc. Am.*, 113(3):1658–1675, 2003.
19. D.S.C. Hui, D.K.L. Choy, F.W.S. Ko, T.S.T. Li, and C.K.W. Lai. Obstructive sleep apnoea syndrome : treatment update. *HKMJ*, 6(2):209–217, June 2000.
20. J.F. Imbert. *Analyse des Structures par Eléments Finis*. Cépaduès Editions, 1991.
21. S. Isono, J.E. Remmers, A. Tanaka, Y. Sho, J. Sato, and T. Nishino. Anatomy of pharynx in patients with obstructive sleep apnea and in normal subjects. *Journal Of Applied Physiology*, 82(4):1319–1326, 1997.

22. O.E. Jensen. Flows through deformable airways. In *Biomathematics Euro Summer School, Dynamical Systems in Physiology and Medicine, Urbino*, 2002. http://www.biomatematica.it/urbino2002/programmi/oejnotes.pdf.
23. J. Krieger, C. Petiau, E. Sforza, T. Weiss, A. Thibault, and A. Bazin. Résisteur de Starling et stabilité du couple sommeil-ventilation. *Neurophysiologie Clinique*, 28:493–506, 1998.
24. W. Kuhlo, E. Doll, and M.C. Franck. Erfolgreiche Behandlung eines Pickwick-Syndroms durch eine Dauertrachealkanüle. *Deutsche Medizinische Wochenschrift*, 94(24):1286–1290, Juni 1969.
25. P.Y. Lagrée, E. Berger, M. Deverge, C. Vilain, and A. Hirschberg. Characterization of the pressure drop in a 2D symmetrical pipe: some asymptotical, numerical and experimental comparisons. *ZAMM (Zeitschrift für Angewandte Mathematik und Mechanik)*, in press.
26. A. Malhotra, Y. Huang, R.B. Fogel, G. Pillar, J.K. Edwards, R. Kikinis, S.H. Loring, and D.P. White. The Male Predisposition to Pharyngeal Collapse. *Am J Respir Crit Care Med*, 166:1388–1395, 2002.
27. A. Malhotra and D.P. White. Obstructive Sleep Apnoea. *The Lancet*, 360:237–245, July 2002.
28. Y. Payan, M. Chabanas, X. Pelorson, C. Vilain, P. Levy, V. Luboz, and P. Perrier. Biomechanical models to simulate consequences of maxillofacial surgery. *C.R. Biologies*, 325:407–417, 2002.
29. X. Pelorson, A. Hirschberg, A.P.J. Wijnands, and H. Bailliet. Description of the flow through in-vitro models of the glottis during phonation. *Acta Acustica*, 3:191–202, 1995.
30. A.N. Rama, S.H. Tekwani, and C.A. Kushida. Sites of Obstruction in Obstructive Sleep Apnea. *Chest*, 122(4):1139–1147, 2002.
31. J.E. Remmers, W.J. De Groot, E.K. Sauerland, and A.M. Anch. Pathogenesis of upper airway occlusion during sleep. *Journal of Applied Physiology*, 44(6):931–938, 1978.
32. R.C. Scherer, D. Shinwari, K.J. De Witt, C. Zhang, B.R. Kucinschi, and A.A. Afjeh. Intraglottal pressure profiles for a symmetric and oblique glottis with a divergence angle of 10 degrees. *J. Acoust. Soc. Am.*, 109:1616–1630, 2001.
33. R.C. Scherer and I.R. Titze. *Vocal Fold Physiology: Contemporary Research and Clinical Issues*, chapter Pressure-flow relationship in a model of the laryngeal airway with diverging glottis, pages 177–193. D.M. Bless and J.H. Abbs (College Hill, San Diego), 1983.
34. H. Schlichting. *Boundary-Layer Theory*. McGraw-Hill Publishing Company, 1979.
35. R.J. Schwab and K.P. Strohl. Pro/Con Editorials. Pro: Sleep Apnea Is an Anatomic Disorder. Con: Sleep Apnea Is Not an Anatomic Disorder. *Am J Respir Crit Care Med*, 168:270–273, 2003.
36. A.H. Shapiro. Steady Flow in Collapsible Tubes. *Journal of Biomechanical Engineering*, 99:126–147, 1977.
37. B. Shome, L.P. Wang, M.H. Santare, A.K. Prasad, A.Z. Szeri, and D. Roberts. Modeling of airflow in the pharynx with application to sleep apnea. *Journal Of Biomechanical Engineering*, 120:416–422, June 1998.
38. P.L. Smith, R.A. Wise, A.R. Gold, A.R. Schwartz, and S. Permutt. Upper airway pressure-flow relationships in obstructive sleep apnea. *Journal Of Applied Physiology*, 64(2):789–795, 1988.
39. W.J. Stronge. *Impact Mechanics*. Cambridge Univ. Press. London, UK., 2000.
40. C.E. Sullivan, F.G. Issa, M. Berthon-Jones, and L. Eves. Reversal of obstructive sleep apnoea by continuous positive airway pressure applied through the nares. *Lancet*, 1:862–865, April 1981.
41. L.R.G. Treloard. *The Physics of Rubber Elasticity (3rd ed.)*. Oxford: Clarendon, 1975.
42. R.E. Walsh, E.D. Michaelson, L.E. Harkleroad, A. Zighelboim, and M.A. Sackner. Upper Airway Obstruction in Obese Patients with Sleep Disturbance and Somnolence. *Annals of Internal Medicine*, 76:185–192, 1972.
43. T. Young, M. Palta, J. Dempsey, J. Skatrud, S. Weber, and S. Badr. The Occurence of Sleep-Disordered Breathing among Middle-Aged Adults. *The New England Journal Of Medicine*, 328(17):1230–1235, April 1993.
44. O.C. Zienkiewicz and R.L. Taylor. *The Finite Element Method. Basic Formulation and Linear Problems*. McGraw-Hill Book Company, 1989.

Appendix 1. Precomputation method

The aim is to obtain $[\mathbf{M}]$ and $\{\mathbf{u_f}^*\}$ that appear in the following relationship:

$$\{\mathbf{u_f}\} = [\mathbf{M}]\{\mathbf{F}\} + \{\mathbf{u_f}^*\}\,. \tag{16}$$

If it is not possible to obtain directly from the Finite Element solver the requiered matrices and vector, the following precomputation method can be applied, based on the fact that any solver will give the value of displacement $\{\mathbf{u_f}\}$ for a given set of forces $\{\mathbf{F}\}$:

1. compute $\{\mathbf{u_f}^*\}$ by application of forces $\{\mathbf{F}\} = \{\mathbf{0}\}$. In the particular case of the latex cylinder, with boundary conditions described in figure 7 (b), $\{\mathbf{u_f}^*\}$ is already known to be $\{\mathbf{0}\}$ since kinematic constraints are immobility constraints.

2. compute $[\mathbf{M}]$. Set $\{\mathbf{F}\} = \{\boldsymbol{\Pi_i}\}$, for each component i of $\{\mathbf{F}\}$, where

$$\{\boldsymbol{\Pi_i}\} = \{0, \ldots, 0, \underbrace{1}_{i^{th} \text{ position}}, 0, \ldots, 0\}^t, \tag{17}$$

   it is clear from (16) that the vector $\left\{\mathbf{u_f}^{\mathbf{i}}\right\}$ obtained is the i^{th} column $\{\mathbf{M}^{\mathbf{i}}\}$ of $[\mathbf{M}]$.

3. build $[\mathbf{M}]$ from all the $\{\mathbf{M}^{\mathbf{i}}\}$ and store it,

Appendix 2. Computation of pressure forces on each element

The aim is to demonstrate how formula (14) is obtained for a discrete pressure distribution on an element. First, from (12), let's explicit $[\mathbf{N}(s,t)]$ for a linear four nodes element:

$$[\mathbf{N}(s,t)] = [\quad Q(-s,-t)\mathbf{I} \quad Q(s,-t)\mathbf{I} \quad Q(s,t)\mathbf{I} \quad Q(-s,t)\mathbf{I} \quad], \tag{18}$$

with

$$Q(s,t) = \frac{1}{4}(1+s)(1+t), \tag{19}$$

and $\mathbf{I}$ the identity matrix of dimension 3 [1]. Since the $\left\{\mathbf{F}^{(e)}_{nodes}\right\}$ is a column vector constituted from the $\left\{\mathbf{F}^{k\,(e)}_{l}\right\}$ vectors, for $(k,l) \in \{-1,1\}$, it is straightforward from (18) and (12) that:

$$\left\{\mathbf{F}_l^{k\,(e)}\right\} = I_l^k \frac{\{\mathbf{a}\}}{4}, \tag{20}$$

with

$$I_l^k = \int_{-1}^{1}\int_{-1}^{1} Q(ks, lt)p(s,t)dsdt. \tag{21}$$

For a discrete pressure distribution $p(s_i, t_j)_{i=1,\ldots,n,\, j=1,\ldots,m}$, with $p(s,t)$ constant on each rectangular element (i,j) of corner coordinates (s_i, t_j) and (s_{i+1}, t_{j+1}), the integral (21) can be rewritten:

$$I_l^k = \sum_{i=1}^{n}\sum_{j=1}^{m} P(s_i, t_j) \int_{s_i}^{s_{i+1}}\int_{t_j}^{t_{j+1}} Q(ks, lt)dsdt. \tag{22}$$

Thanks to formula (19) which explicits Q, this last integral can be expressed analytically:

$$\int_{s_i}^{s_{i+1}}\int_{t_j}^{t_{j+1}} Q(ks, lt)dsdt = \frac{1}{4}\int_{s_i}^{s_{i+1}}\int_{t_j}^{t_{j+1}} (1+ks)(1+lt)dsdt = \frac{1}{4}\int_{s_i}^{s_{i+1}}(1+ks)ds\int_{t_j}^{t_{j+1}}(1+lt)dt. \tag{23}$$

The last two separate integrals are easy to compute (areas of trapezoids), so that:

$$\int_{s_i}^{s_{i+1}}\int_{t_j}^{t_{j+1}} Q(ks, lt)dsdt = \frac{kl}{4}\omega(ks_i, ks_{i+1})\omega(lt_j, lt_{j+1}), \tag{24}$$

with $\omega(x, y)$ the function given in (15). Finally,

$$I_l^k = \frac{kl}{4}\sum_{i=1}^{n}\sum_{j=1}^{m} P(s_i, t_j)\omega(ks_i, ks_{i+1})\omega(lt_j, lt_{j+1}). \tag{25}$$

From (20) and (25), (14) is then obtained.

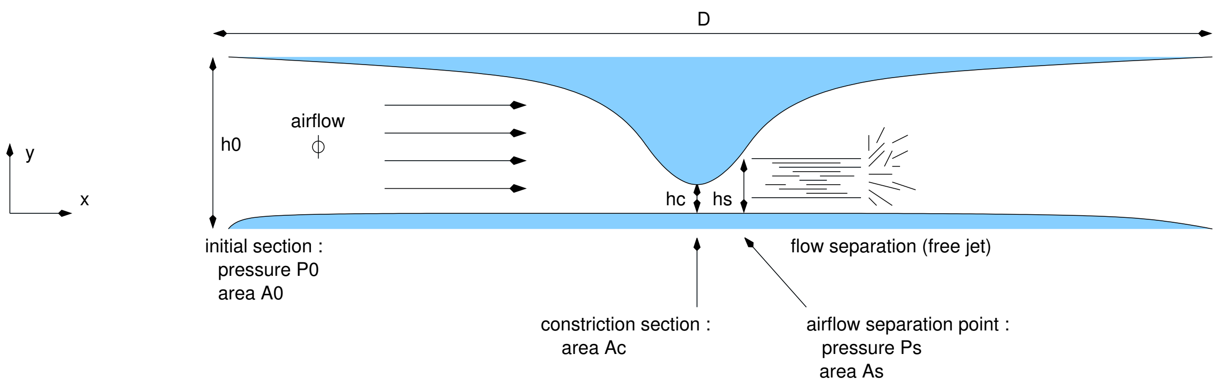

Fig. 1. *Flow inside a constriction.*

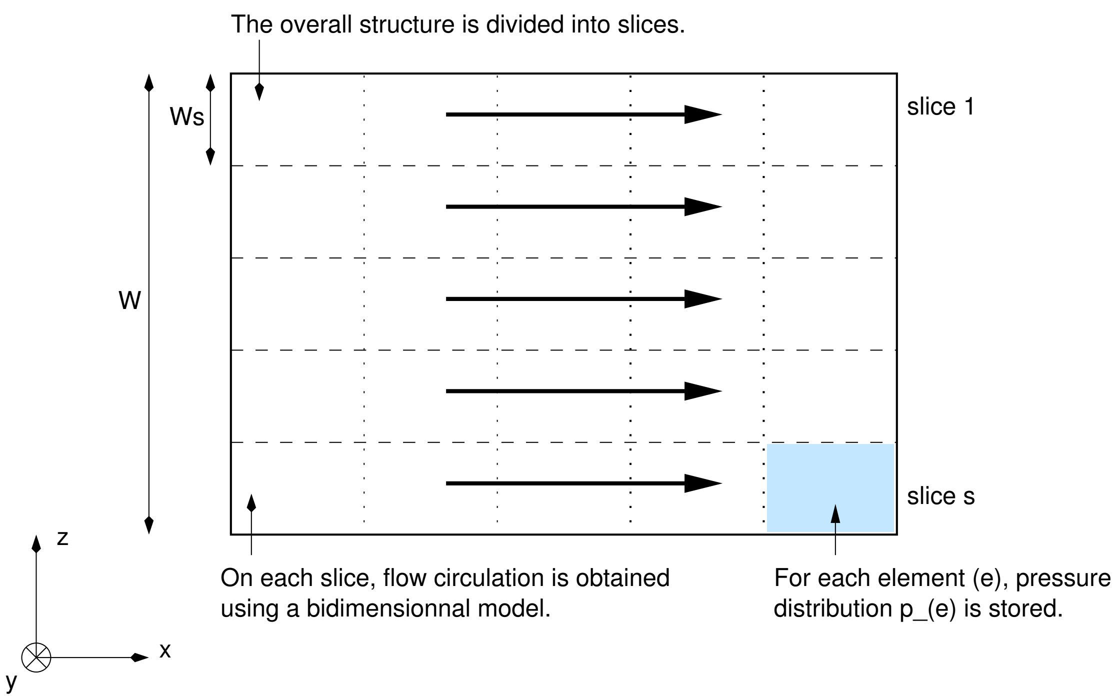

Fig. 2. *Division of the structural model into slices for flow computation.*

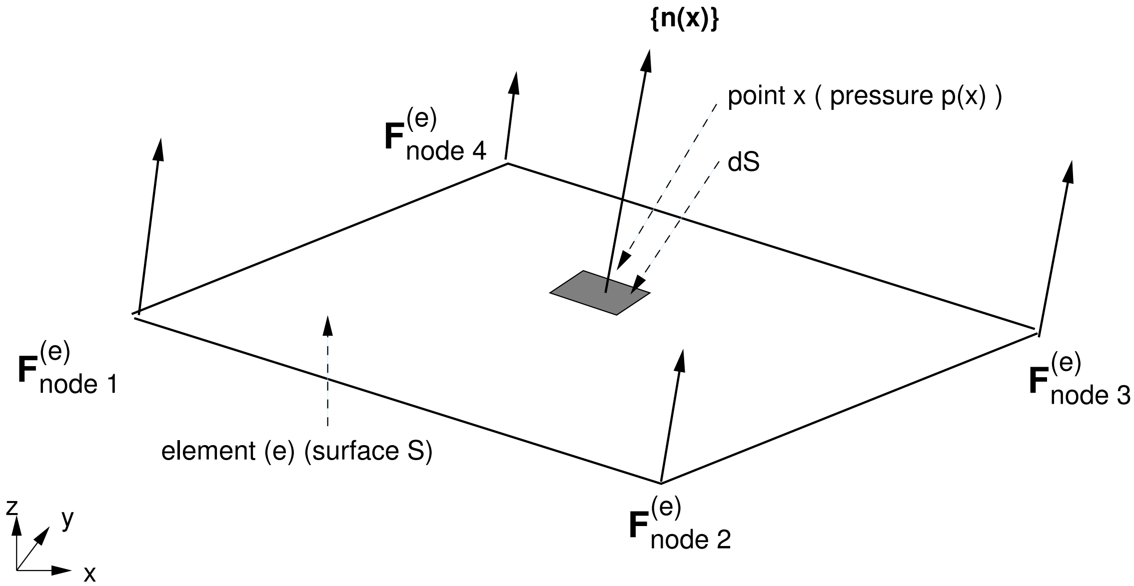

Fig. 3. *Pressure and equivalent nodal forces on an element* (e). $\left\{\mathbf{F}^{(e)}_{nodes}\right\}$ *is constituted of* $\mathbf{F}^{(e)}_{node\ 1}$, $\mathbf{F}^{(e)}_{node\ 2}$, $\mathbf{F}^{(e)}_{node\ 3}$, $\mathbf{F}^{(e)}_{node\ 4}$.

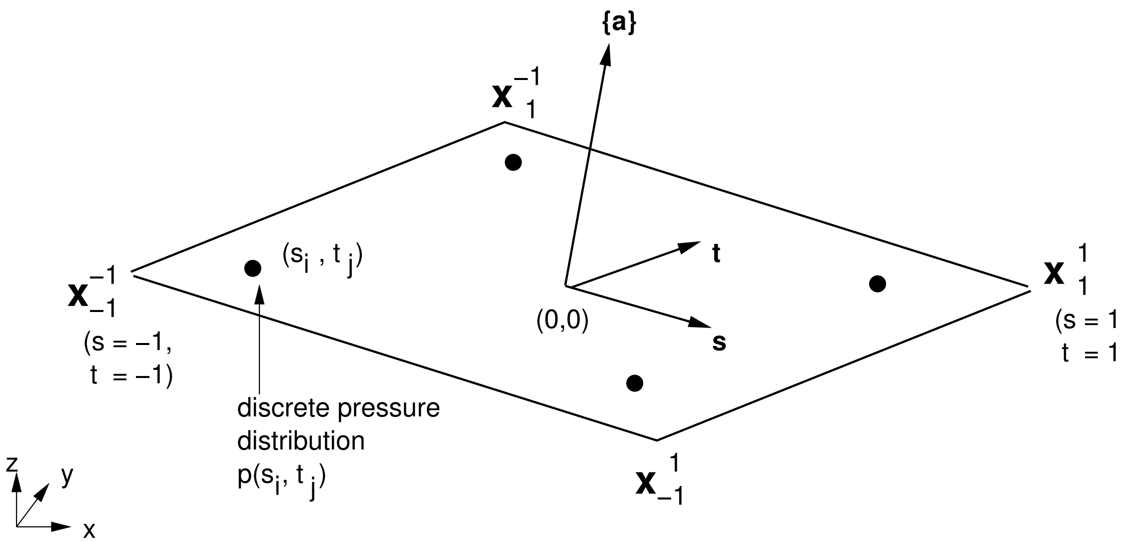

Fig. 4. *Standard coordinate system associated to an element (e).*

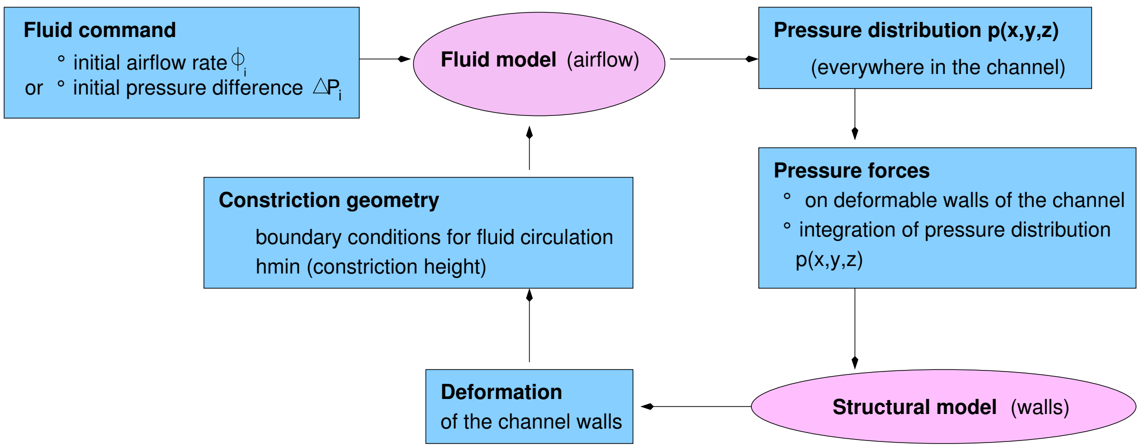

Fig. 5. *The general algorithm used for coupling fluid and structure.*

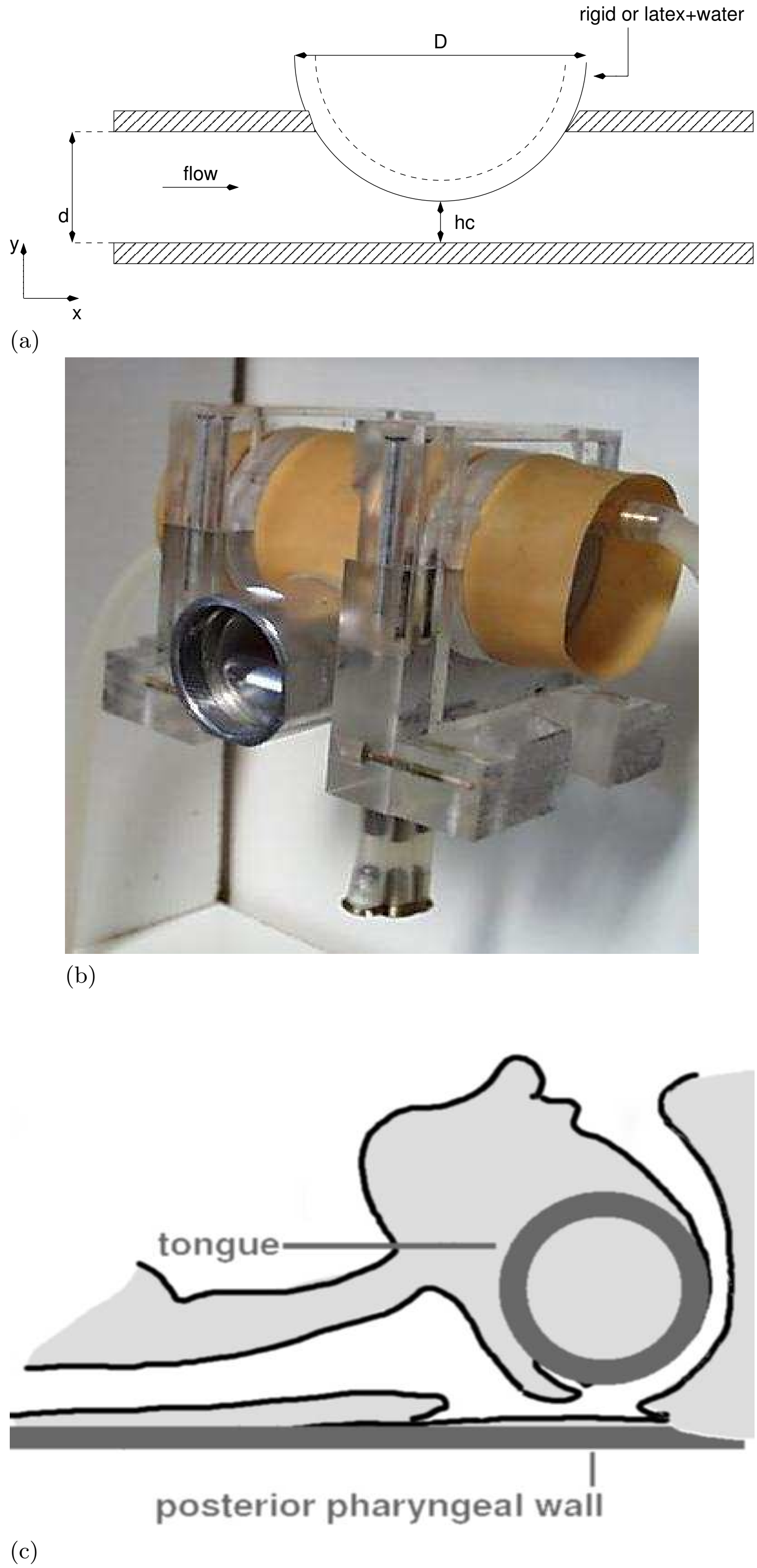

Fig. 6. *(a) Diagram and (b) photography of the in-vitro setup. (c) Sagittal view of the upper airway.*

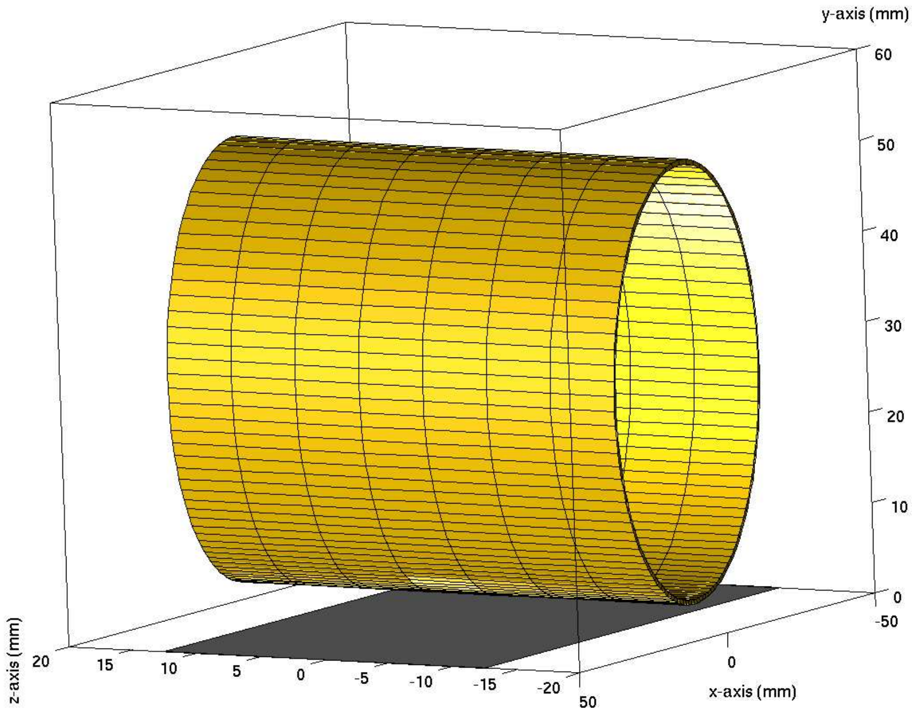

(a)

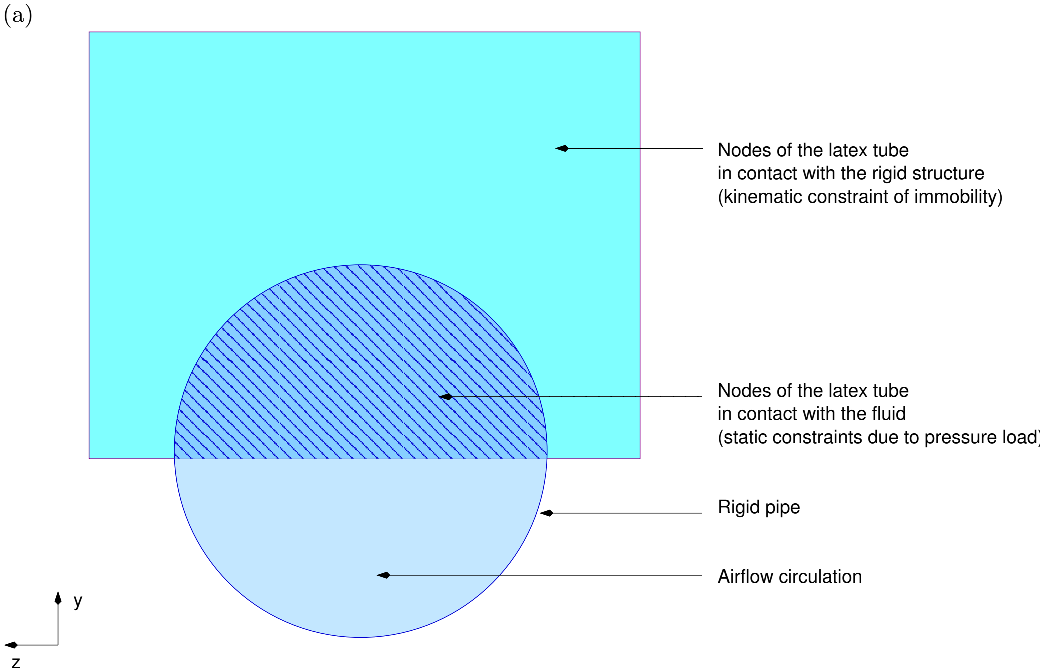

(b)

Fig. 7. *(a) Model of the in-vitro setup. (b) Boundary conditions associated to the latex tube.*

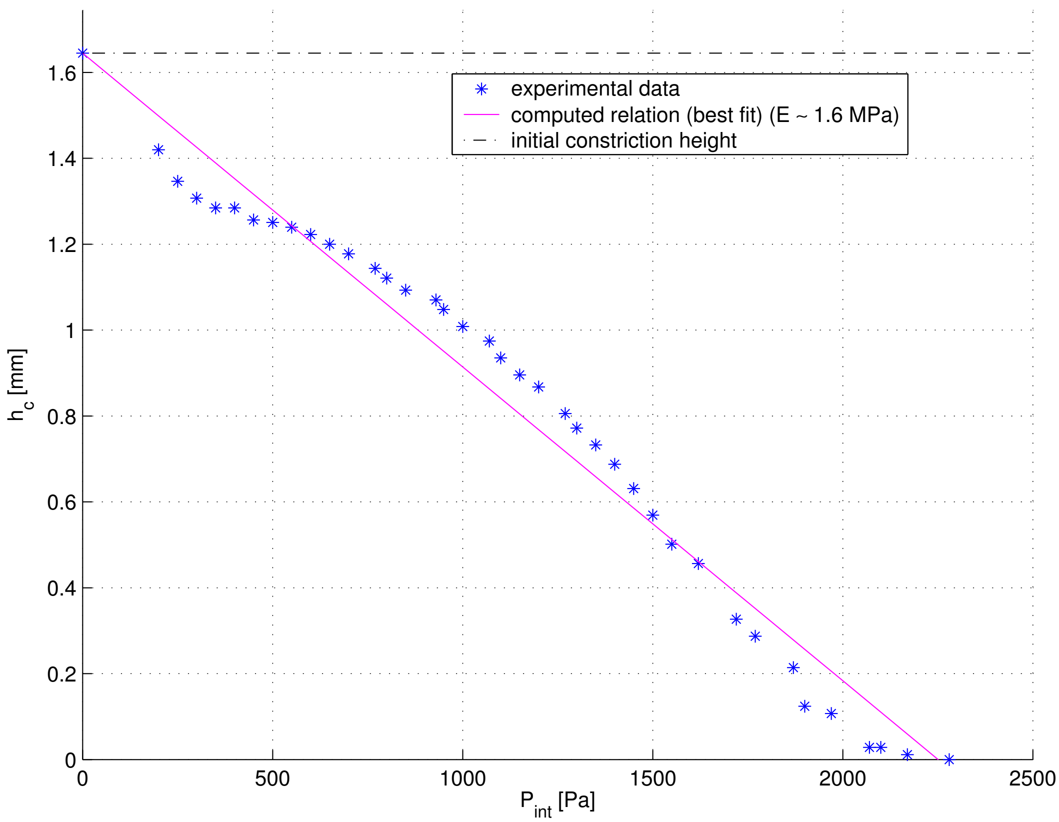

Fig. 8. *Variations of the constriction height h_c in response to variations of the internal pressure P_{int}.*

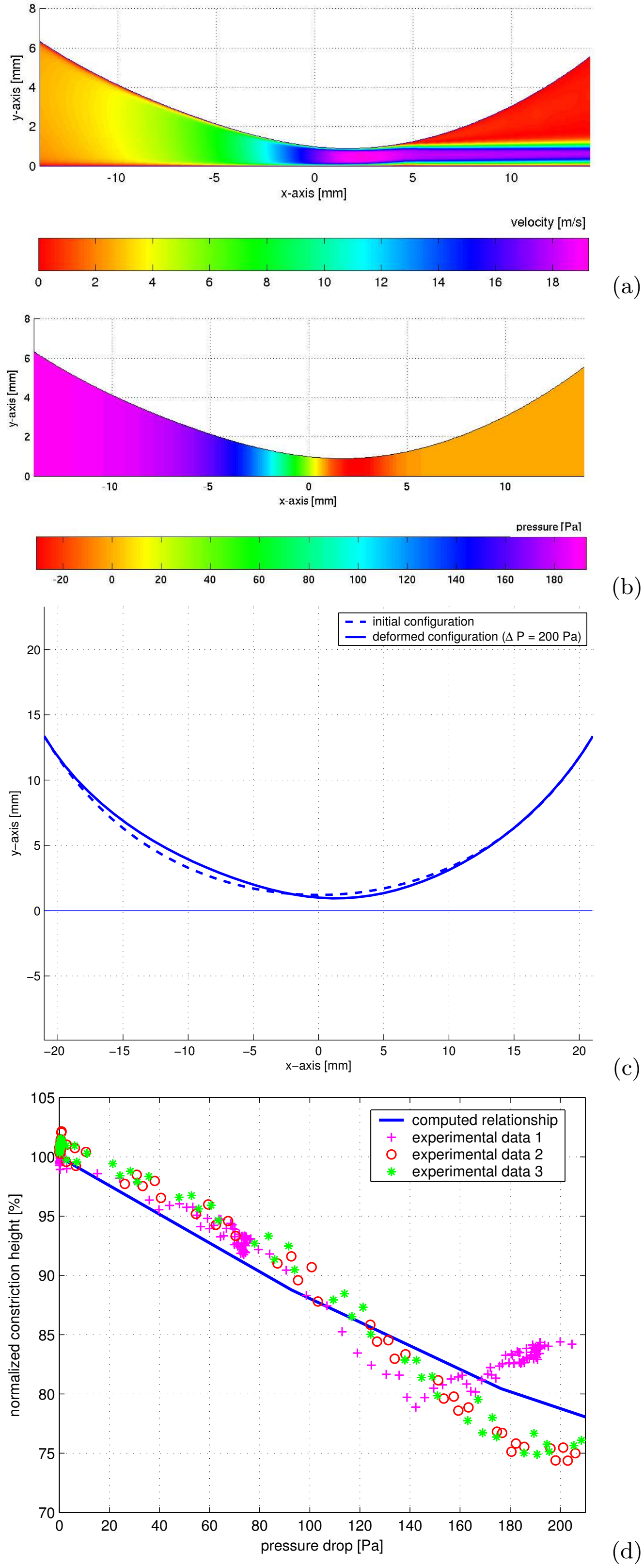

Fig. 9. *Simulation of a hypopnea, for $\Delta P = 210$ Pa, $P_{int} = 200$ Pa and $h_c = 1.2$ mm. (a) Velocity profile (absolute value). Note the acceleration of the fluid while entering the constriction. Flow separation and jet formation are observed. (b) Pressure distribution. Note the negative pressure at the level of the constriction. (c) Lateral view of the latex tube, in initial position (dashed line) and after computation of the deformation (solid line). (d) Constriction height variation in response to inlet pressure. Comparison of theoretical and experimental values.*

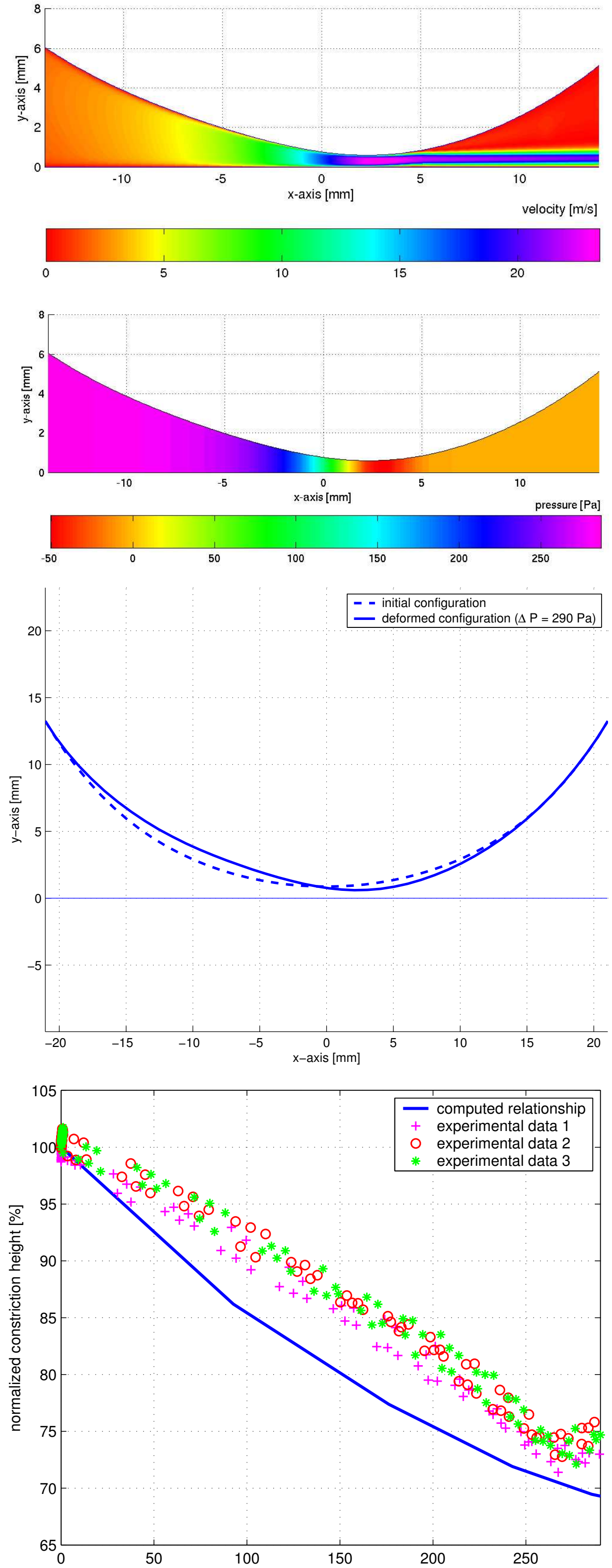

(a)

(b)

(c)

(d)

Fig. 10. *Simulation of a hypopnea, for $\Delta P = 290$ Pa, $P_{int} = 400$ Pa and $h_c = 0.87$ mm. (a) Velocity profile (absolute value). (b) Pressure distribution. (c) Lateral view of the latex tube, in initial position (dashed line) and after computation of the deformation (solid line). (d) Constriction height variation in response to inlet pressure. Comparison of theoretical and experimental values.*

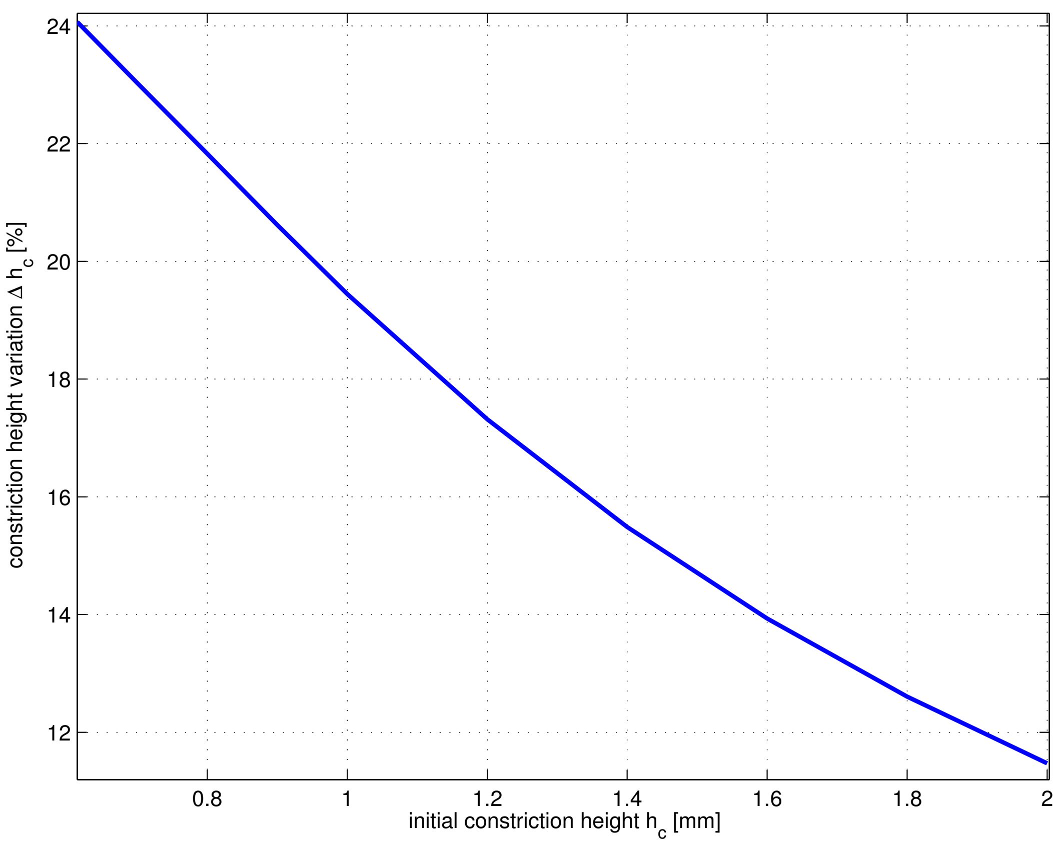

Fig. 11. *Influence of the initial constriction height h_c on the partial closure of the channel. Simulations with parameters : ΔP = 150 Pa, P_{int} = 200 Pa, E = 1.6 MPa.*

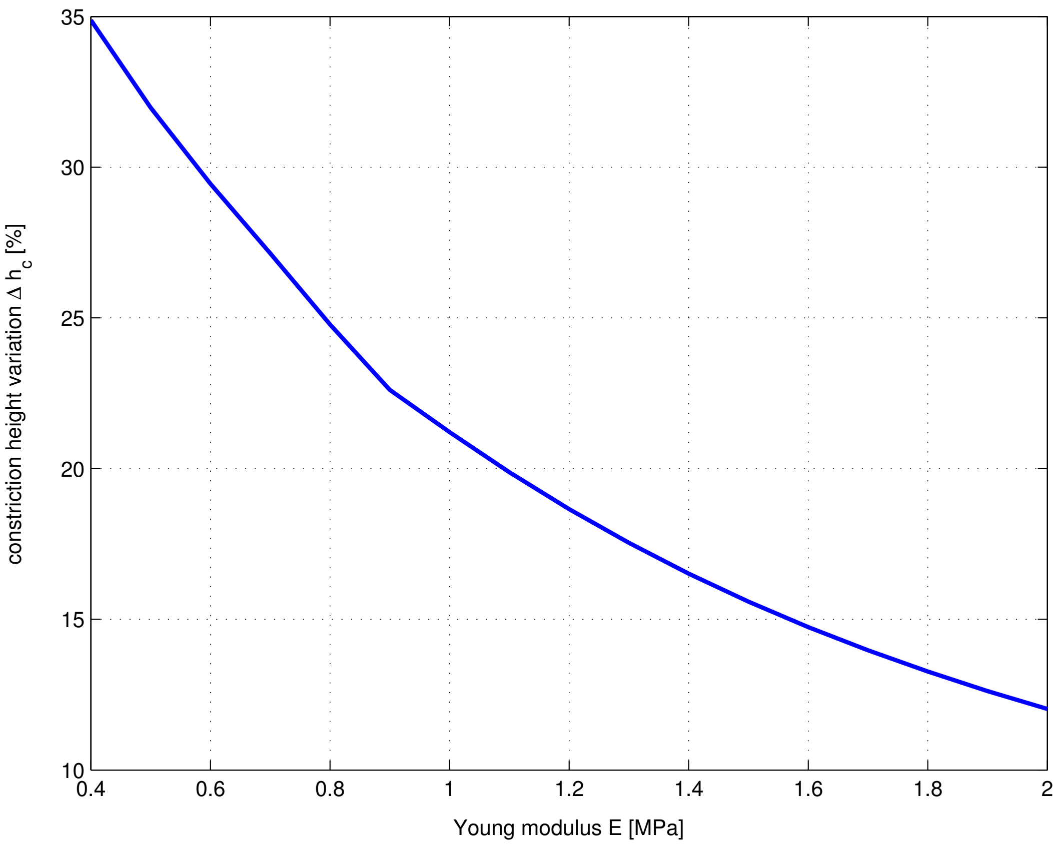

Fig. 12. *Influence of the Young modulus E on the partial closure of the channel. Simulations with parameters : ΔP = 150 Pa, P_{int} = 200 Pa, h_c = 1.5 mm.*

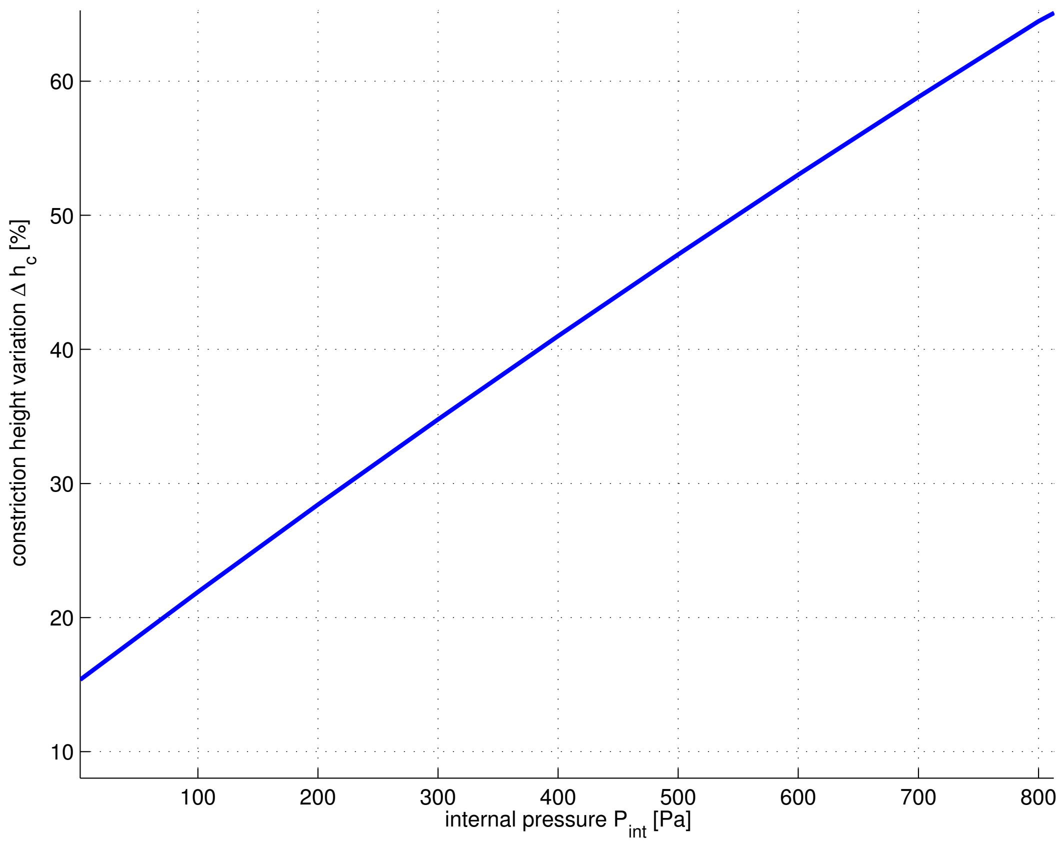

Fig. 13. *Influence of the internal pressure P_{int} on the partial closure of the channel. Simulations with parameters : ΔP = 150 Pa, h_c = 1.5 mm, E = 1.6 MPa.*